First publ. in: Journal of Chemical Physics 114 (2001), 22, pp. 10094-10104

Measurement of surface charge densities on Brownian particles using total internal reflection microscopy

H. H. von Grünberg, L. Helden, P. Leiderer, and C. Bechinger
Fakultät für Physik, Universität Konstanz, 78457 Konstanz, Germany

(Received 28 December 2000; accepted 21 March 2001)

Due to double-layer forces a charged colloid suspended in an electrolyte is repelled from a like-charged planar wall. We demonstrate that and how a precise measurement of these double-layer forces acting on a colloid near a glass surface can be used to determine surface charge densities. The effective wall–colloid potentials are measured using the total internal reflection microscopy technique, and a whole series of such potentials, taken for various different salt concentrations, are then analyzed in terms of a given theoretical interaction potential, where the surface charge densities are the only unknown parameters. We find reasonable values for the surface charge densities of silica and polystyrene spheres in water, and compare the proposed method with other more established techniques to measure surface charge densities on single particles.

I. INTRODUCTION

Interactions that occur between charged objects immersed in an electrolytic solution, such as colloids, micelles, vesicles, and proteins, play an important role in many biological and physicochemical systems.[1,2] In the vicinity of charged surfaces in solution, a diffuse layer of electrolyte ions forms, with a thickness in the order of the Debye screening length κ^{-1}. Accordingly, if two such objects having like-charged surfaces approach each other closely, their double layers start to overlap which eventually leads to an increase of counter-ion density in the gap between them relative to the bulk solution. This results in a repulsive double-layer force[2,3] being—besides dispersion and steric interactions—one of the principal long-range forces in such systems.

Besides its importance for the stabilization of charged colloidal suspensions, double-layer forces are also crucial for the interpretation of ion adsorption and ion permeation processes (see, e.g., Ref. 4) and for the understanding of mechanical properties of biological membranes, the latter being important in, e.g., membrane–membrane interactions and ensuing properties like bacterial adhesion.[5] The details of such double-layers depend crucially on the surface charge density of the charged object. In addition, surface charge densities are also interesting because they contain important structural and chemical information of surfaces which might lead to conclusions about the composition of such interfaces. This article therefore concentrates on surface charge densities and proposes a new and simple method how to determine such charge densities.

Different methods have been suggested to measure the surface charge or the surface potential of an object. Measurements of the velocity of charged objects in the presence of electric fields, e.g., allow the determination of the so-called ζ-potential. Several methods to determine the ζ-potential like electrophoresis, electro-osmosis, streaming potential and sedimentation potential are well established.[6] Common to all these techniques, however, is that considerable theoretical input is required; in particular, one needs the relation between the velocity response of the particle to an external field and its surface potential, which usually requires a solution of the Smoluchowski equation. Another disadvantage of dynamical measurements in general is that, since the hydrodynamic radius of the particle is not known *a priori*, the exact relationship between the static surface potential and the dynamically determined ζ potential is often not clear.

Other approaches utilize the fact that surface charges can be obtained from a measurement of double-layer forces. Probably the best known technique to study double layer repulsion forces is the surface force apparatus (SFA) which has been developed by Israelachvili and Adams.[1] However, while this technique has been very successful in the determination of double-layer, solvation and steric forces, it is experimentally limited to macroscopic bodies, i.e., typically two crossed mica cylinders. In contrast, the direct measurement of interaction forces between a single colloidal particle and a wall is difficult if not impossible to achieve with the SFA. To overcome that limitation, it has been suggested to measure double-layer forces close to a flat surface by attaching a colloidal sphere to the tip of an atomic force microscope (AFM) cantilever, see Refs. 7–9. In the first experiment of this kind Ducker *et al.*[7] measured the forces between a 3.5 μm silica sphere attached to an AFM cantilever and a silicon wafer in aqueous solutions for various concentrations of NaCl salt and showed consistency with DLVO-theory in the regime of 5–40 nm distance to the surface. Common to all AFM-based techniques is the restriction to very small separations where forces are strong enough to cause a detectable bending of the cantilever. At larger separations, however, (where dispersion forces are negligible) double-layer forces are too weak to be measured with AFM.

Another method that allows measurements on single unperturbed Brownian particles is total internal reflection microscopy (TIRM) which has been introduced by the group of

Prieve.[10–12] TIRM is based on the scattering of a single particle that moves inside an evanescent field which is formed at an interface by total reflection of a laser beam. It has been demonstrated by several groups that TIRM allows the precise determination of double-layer repulsion potentials between a particle and a flat wall. For thin, slightly overlapping ion clouds, the double-layer interaction potential of a spherical particle at a distance h above a charged planar wall, is given by a simple exponential function $e^{-\kappa h}$, with the screening parameter κ given by the salt concentration in the system. Indeed, such an exponential dependence of the double-layer repulsion has been found in several experiments employing TIRM.[33–35] A precise determination of surface charges or surface potentials, however, is difficult when using the standard data evaluation of TIRM.

In the present paper we introduce a more elaborate method to analyze TIRM data which additionally considers that the prefactor of the exponential function in the wall–colloid interaction potential is not constant, but a complex function of κ. The purpose of this paper is to show that accurate values for surface charge densities can be obtained if the kappa dependence is carefully analyzed. This opens up a convenient way to measure surface charges via double-layer forces on a single particle which may complement other more established methods like those mentioned above. Besides a good estimate of the surface charges of wall and colloid, our data represent a direct experimental confirmation of the theoretical wall–colloid interaction potential which has been originally suggested by Verwey and Overbeek.[13] In the theoretical section of this paper, we interpret this wall–colloid potential as resulting from the interaction of a point-charge with the unperturbed double-layer in front of the charged wall. The point-charge representing the colloid can thus be regarded as a test charge which probes the unperturbed double-layer. Seen in this way, our measurement of the effective wall–colloid interaction potential can also be understood as an indirect measurement of the unperturbed double-layer. This double-layer in front of a planar wall can be calculated from the nonlinear Poisson–Boltzmann equation, one of the very few cases where this can be done analytically. This approach, known as the Gouy–Chapman solution,[14] belongs to the fundamental building blocks of the classical theory on double-layer forces.

The paper is organized as follows: First we derive the effective interaction between a colloidal sphere and a flat wall from the grand canonical potential. Applying approximations suitable for our experimental range of parameters results in an analytic expression for the interaction potential as a function of surface charges, Debye length, and separation distance. Then the principles of TIRM are reviewed and the relation between surface charge and measured potentials is clarified. Next the experimental results are presented and compared with our theoretical predictions. It follows the central idea of this work, the determination of surface charge densities from interaction potentials. After a brief discussion of our results, we conclude with a short summary of the main points of this paper.

II. EFFECTIVE WALL–COLLOID INTERACTION

A. Poisson–Boltzmann theory

In this theory section, we seek to calculate the effective interaction between two like charged objects, a spherical colloid and a planar wall, both immersed in an unbounded 1:1 electrolyte solution. The sphere of radius a bears Z negative charges e at its surface, while the confining wall has a surface charge density of $-e\sigma_W$. The distance from the center of the sphere to the surface of the wall is h. In the vicinity of these objects, the net charge density distribution $\rho(\mathbf{r}) = \rho_+(\mathbf{r}) - \rho_-(\mathbf{r})$ of the electrolyte ions is inhomogeneous. In a mean-field approach, the density distribution of both the positive and negative (monovalent) ions $\rho_\pm$ are related to the normalized electrostatic potential Φ through $\rho_\pm = \rho_s e^{\mp\Phi}$. Far away from both surfaces, $\rho_\pm$ approach their bulk value ρ_s so that $\rho(\mathbf{r})$ then vanishes. The potential Φ is the solution to the Poisson–Boltzmann (PB) equation[15]

$$\nabla^2\Phi = \kappa^2 \sinh\Phi, \tag{1}$$

where $\kappa^2 = 8\pi\lambda_B\rho_s$ is the screening parameter characterizing the electrolyte solution, $\lambda_B = e^2\beta/\epsilon$ the Bjerrum length ($\beta = 1/kT$), and ϵ the dielectric constant of the solvent.

The charges on the surface of the sphere and the interface enter the calculation through the boundary conditions. Let us call ∂G_w the boundary given by the interfacial wall at $z=0$, ∂G_C the surface of our colloid and G the region of the electrolytic solution between both surfaces. At ∂G_C we then require the normal component of the electric field to be equal to the colloidal surface-charge density $\sigma_C = Z/4\pi a^2$ (constant-charge boundary condition), while at ∂G_W we are faced with the more complicated boundary condition,

$$\epsilon\partial_z\Phi|_{z=0+} - \epsilon'\partial_z\Phi|_{z=0-} = 4\pi\epsilon\lambda_B\sigma_W, \tag{2}$$

where ϵ' is the dielectric constant of the wall material at $z \leqslant 0$. In general, this boundary condition is not easy to satisfy in a PB problem, even in a full numerical treatment.[16] Since we are here concerned with an aqueous electrolyte solution having a dielectric constant ($\epsilon = 78$) that is more than an order of magnitude larger than the dielectric constant ϵ' of practically every possible wall material, we may assume $\epsilon'/\epsilon \to 0$. We then know the absolute value of the electric field at $z=0$ to be given by σ_W. Using this approximation, we here consider a limit where image charges are fully switched on.[17] Our first task thus is to solve the following boundary value problem (BVP),

$$\begin{aligned} &\nabla^2\Phi(\mathbf{r}) = \kappa^2\sinh\Phi(\mathbf{r}), && \mathbf{r}\in G,\\ &\mathbf{n}_W\nabla\Phi = 4\pi\lambda_B\sigma_W, && \mathbf{r}\in\partial G_W,\\ &\mathbf{n}_C\nabla\Phi = 4\pi\lambda_B\sigma_C, && \mathbf{r}\in\partial G_C, \end{aligned} \tag{3}$$

where $\mathbf{n}_W$ and $\mathbf{n}_C$ are two unit vectors directed normal to the surfaces of wall and colloidal sphere, respectively, and pointing into the region G. The position of the boundary ∂G_C in Eq. (3) still depends on the distance h between the colloid and the wall. For one specific value of h, we have one BVP to solve. In the following, we write Φ_h whenever we want to stress that Φ depends on the parameter h. Once we know

Φ_h, we can compute the grand potential of our system (since the electrolyte solution is unbounded we work in the grand-canonical ensemble),

$$\beta\Omega_h=\frac{1}{8\pi\lambda_B}\int_G d\mathbf{r}(\nabla\Phi_h)^2 + \sum_{\alpha=\pm}\int_G d\mathbf{r}\rho_\alpha(\log\rho_\alpha\Lambda^3-1) - \int_G d\mathbf{r}(\beta\mu_s(\rho_+ +\rho_-)-2\rho_s)-\beta W^{\mathrm{SE}}, \quad (4)$$

which by substitution of $\rho_\pm=\rho_s e^{\mp\Phi_h}$ and $\beta\mu_s=\log\rho_s\Lambda^3$ becomes

$$\beta\Omega_h=\frac{1}{8\pi\lambda_B}\int_G d\mathbf{r}[(\nabla\Phi_h)^2 + 2\kappa^2(\Phi_h\sinh\Phi_h-\cosh\Phi_h+1)]-\beta W^{\mathrm{SE}}. \quad (5)$$

The last term, $\beta W^{\mathrm{SE}}=Z^2\lambda_B/2a$, is the Coulomb self-energy of the colloidal charges, which we have subtracted for later convenience. Through Φ_h the grand potential is, of course, also dependent on the parameter h. The effective wall–colloid interaction potential $\beta V(h)$ can now be defined as the total change of the grand potential when the colloidal sphere is brought from ∞ to a finite distance h. Hence,

$$\beta V(h)=\beta(\Omega_h-\Omega_\infty). \quad (6)$$

With the numerical solution of Eq. (3) inserted in Eqs. (5) and (6), we have thus arrived at the effective interaction potential in full nonlinear PB theory. Our technique to solve Eq. (3) (subtraction of Gouy–Chapman solution, bispherical coordinates) is described elsewhere.[18]

B. Approximate interaction potentials

If the normalized potential Φ is smaller than one everywhere, we may linearize the differential equation in Eq. (3). The resulting BVP can be solved in the limit $\kappa a\to 0$ (point-like colloid), and Eqs. (5) and (6) then result in the effective interaction potential in linear theory (see Appendix),

$$\beta V(h)=-Z\Phi_1(z)\big|_{z=\infty}^{z=h}+\frac{Z^2\lambda_B}{2}\frac{e^{-2\kappa h}}{2h}. \quad (7)$$

Here Φ_1 is the potential of a double-layer of an isolated wall, which in linear theory is

$$\Phi_1(z)=-4\pi\frac{\lambda_B\sigma_W}{\kappa}e^{-\kappa z} \quad (8)$$

[see Eq. (A7)]. The interpretation of Eq. (7) is obvious: The first term, dominating for large h and strong interfacial charges, is just the electrostatic energy of a point-charge $-Ze$ interacting with the unperturbed double-layer of the charged wall, while the second term is the screened interaction between the point-charge $-Ze$ at the position $z=h$ and its own image charge being located at $z=-h$. Their distance hence is $2h$ which explains the factor 2 in front of the wall–sphere distance h in Eq. (7), see Ref. 19 for the explanation of the prefactor.

For our purposes, Eq. (7) cannot be used as it stands, but requires two modifications. The first of these concerns Eq. (8), the potential of the isolated wall in linear approximation. This is correct if $\Phi<1$, which is valid in a very small region of the parameter space only. A simple remedy for this deficiency is to replace Φ_1 of Eq. (8) by the well-known Gouy–Chapman solution to the nonlinear PB problem of a double-layer near a planar charged wall,[2]

$$\Phi_1(z)=4\,\mathrm{arctanh}\,(e^{-\kappa z}\tanh(\Phi_W/4)), \quad (9)$$

where Φ_W is the wall surface potential. The derivative of this potential with respect to z at $z=0$ is, $-2\kappa\sinh\Phi_W/2$, which according to Eq. (3) must be equal to $4\pi\lambda_B\sigma_W$. This leads to the Graham-equation[2,1] relating surface charge densities to surface potentials,

$$4\pi\lambda_B\sigma_{W/C}=-2\kappa\sinh(\Phi_{W/C}/2). \quad (10)$$

The two subscript C and W are introduced, because this expression will be used for the surface-charge/surface-potential relation of both the colloidal (subscript C) and the wall (subscript W) surface. For a convenient notation, we use Eq. (10) to define the following two γ factors:

$$\gamma_{W/C}=\left|\tanh\Phi_{W/C}/4\right|=\tanh\left[\frac{1}{2}\mathrm{arcsinh}\left(\frac{2\pi\lambda_B\sigma_{W/C}}{\kappa}\right)\right], \quad (11)$$

which we will view as a function of κ^{-1}, further below. If $\kappa z>1$, Eq. (9) becomes

$$\Phi_1(z)=-4\gamma_W e^{-\kappa z}, \quad (12)$$

because γ_W cannot be larger than one.

The second modification concerns the limit $\kappa a\to 0$ which is certainly not realized in our experiment. We here may replace the bare colloidal charge by a renormalized (or effective) charge, a heuristic procedure which is well-known from the theory of effective colloid-colloid interaction in bulk.[20] Equation (7) may then be used also for finite values of κa provided one replaces the bare Z by

$$Z_{\mathrm{eff}}=\frac{Ze^{\kappa a}}{1+\kappa a}. \quad (13)$$

If in addition to this finite size effect, the surface charge density of the colloidal particle is too high for the linearization approximation to hold, one may hope to capture some nonlinear effects by representing the spherical double-layer around the colloid by that of a planar wall, Eq. (12). Formally, this can be done by renormalizing the charge yet another time, thus replacing Z by

$$Z_{\mathrm{eff}}=\frac{a}{\lambda_B}4\gamma_C e^{\kappa a}, \quad (14)$$

see Ref. 21.

Inserting now the effective charges of Eqs. (13) and (14) and the potential of Eq. (12) into Eq. (7), we finally obtain two expressions for the effective wall–colloid interaction, which are valid in different regions of the $(\kappa a,\kappa h)$-plane. These are

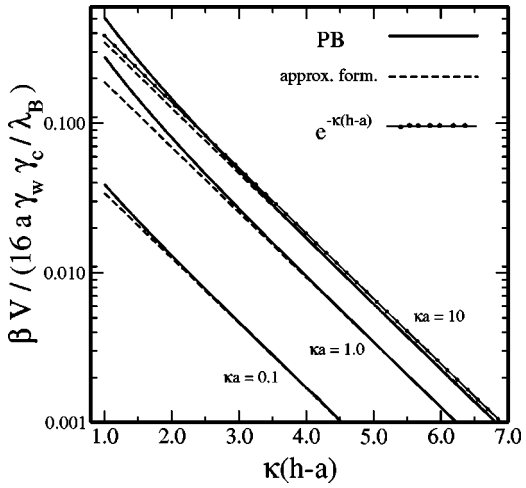

FIG. 1. Colloid–wall interaction potentials in reduced units, calculated for three different colloidal sphere radii. The accuracy of two approximate potentials Eqs. (15) (dashed lines) and (16) (line with filled circles), are tested against the potential that is based on the solution to the full nonlinear Poisson–Boltzmann equation (thick solid line).

$$\beta V(h) = \frac{Ze^{\kappa a}}{1+\kappa a}\left[4\gamma_W e^{-\kappa h} + \frac{Ze^{\kappa a}}{1+\kappa a}\frac{\lambda_B}{2}\frac{e^{-2\kappa h}}{2h}\right] \qquad (15)$$

and

$$\beta V(h) = 4\frac{ae^{\kappa a}}{\lambda_B}\gamma_C[4\gamma_W e^{-\kappa h} + \gamma_C e^{\kappa a}e^{-2\kappa h}]. \qquad (16)$$

The conventional way to derive Eq. (16)—briefly outlined in the appendix—is more direct[13] making use of the well-known Derjaguin approximation. However, we emphasize that this derivation gives only the first term in Eq. (16), while ours leads also to the image-charge interaction terms [second term in Eqs. (15) and (16)].

C. Experimentally accessible interaction potentials

We give a more elaborate derivation of these potentials in Ref. 18, where we have also carefully tested in what region of the four-dimensional parameter space $(\kappa a, \kappa h, \sigma_W, \sigma_C)$ these potentials represent a reliable approximation of the potentials based on the exact solution to the nonlinear PB equation. To check if and how good Eqs. (15) and (16) work in our specific case, let us concentrate here on a set of parameters that are typically realized in our experiments (cf. data plots further below). These parameters are: $\lambda_B = 0.72\,\text{nm}$, $\kappa^{-1} = 100\,\text{nm}$, $\sigma_W = 0.0007\,\text{C/m}^2$, $\sigma_C = 0.0001\,\text{C/m}^2$, and $\kappa(h-a)$ ranging approximately between 2 and 10 in our experiment. Using these values in Eqs. (3), (5), and (6), we calculate the interaction potential in PB theory and compare it with the approximate potentials of Eqs. (15) and (16) in Fig. 1.

Shown in this figure are the interaction potentials in a logarithmic plot for three different values of κa. To facilitate a direct comparison, we have divided $\beta V(h)$ by the prefactor of the first term of the potential in Eq. (16), $16a\gamma_C\gamma_W/\lambda_B$, and plotted it as a function of $\kappa(h-a)$. Plotted in this way, the potentials of Eq. (16) for all three values of κa collapse onto the same straight line (line with filled circles in Fig. 1), which shows that the image-charge term of Eq. (16) is insignificant in our parameter regime. Without this term Eq. (16), divided by the factor $16a\gamma_C\gamma_W/\lambda_B$, then reduces to the same exponential function $e^{-\kappa(h-a)}$ for all three values of κa. The dashed lines in Fig. 1 are the interaction potentials obtained from Eq. (15), which show for all three values of κa good agreement with the PB based interaction potential over a remarkably large $\kappa(h-a)$ range. It is evident from this figure that with increasing κa both the PB based interaction potential as well as the interaction potential of Eq. (15) approach the straight line corresponding to the interaction potential in Eq. (16). Closer inspection of the prefactors in Eqs. (15) and (16) show that for our value of σ_C both interaction potentials become identical in the limit $\kappa a \to \infty$.

We can draw two conclusions from Fig. 1. First, for $\kappa a > 10$ and $\kappa(h-a) > 2$, the difference between the full PB interaction potential and the approximate expressions of Eqs. (15) and (16) is marginal. Since, in all our measurements the value of κa remains always well above 10, both interaction potentials Eqs. (15) and (16), are reasonably good under our experimental conditions. In the following, we will use Eq. (16). We, secondly, realize that image charge effects in our parameter regime are not to be expected; we therefore may drop the second term in Eq. (16).

So far, we have only considered the contribution of the double-layer force to the effective wall–sphere interaction potential. In our experiment we study a colloidal sphere which is located at the bottom of a glass container, and which is thus pressed by gravitational forces against the double-layer. The gravitation potential reads

$$\beta V_{\text{grav}}(h) = \frac{4\pi a^3}{3} g(\rho_{\text{sph}} - \rho_w)(h-a) = G_{\text{eff}}(h-a), \qquad (17)$$

with ρ_{sph} and ρ_w being the density of the sphere and of water, respectively. Another contribution to the total potential comes from the short-ranged dispersion interaction, which in our experiment, however, is important only under high salt conditions. We take Hamaker's linear superposition formula,[1]

$$\beta V_{\text{disp}}(h) = -\frac{A(h)}{6}\left\{\frac{2a}{h}\frac{h+a}{h+2a} - \log\frac{h+2a}{h}\right\}, \qquad (18)$$

which Bevan and Prieve[22] successfully used to interpret their TIRM data of sphere–wall interaction potentials in the high-salt limit. The retarded, screened Hamaker constant $A(h)$ has been calculated according to Bevan and Prieve.[22] Both contributions, Eqs. (18) and (17), are to be subtracted from our measured potential in order to extract the double layer interaction potential which—after all the considerations of this section—we expect to obey the following simple relation:

$$\beta V(h) = \frac{16a}{\lambda_B}\gamma_C\gamma_W e^{-\kappa(h-a)}. \qquad (19)$$

The prefactor of the exponential in Eq. (19) depends on κ and thus on the salt concentration of the electrolyte solution. We see from Eq. (11) that the prefactors of double-layer potentials at different salt concentrations are interconnected, with the only open parameter being the surface charge den-

sity of the wall and the sphere, σ_W and σ_C. This brings us to the main point: If we measure a sequence of interaction potentials for a variety of different salt concentrations and extract the double layer contribution, we can determine σ_W and σ_C by a systematic analysis of the κ dependence of the prefactors in Eq. (19). This is the central idea of this paper.

III. THE EXPERIMENT

Double-layer potentials have been measured by using TIRM, which has been described and reviewed in a number of previous publications and will here discussed only in brief.[10–12] When light is totally reflected at an interface an evanescent field is created whose intensity I decays exponentially with distance z perpendicular to the interface,

$$I(z)=I_0 e^{-\xi z}, \tag{20}$$

where I_0 is the intensity of the evanescent wave at the interface ($z=0$) and ξ is the inverse characteristic penetration depth of the evanescent wave,

$$\xi=\left[\frac{\lambda/n_1}{4\pi(\sin^2\Theta-(n_2/n_1)^2)^{1/2}}\right]^{-1} \tag{21}$$

with λ the wavelength of light in vacuum, Θ the angle of incidence, and n_1 and n_2 being the refractive indices of the solvent–glass interface. If a colloidal sphere of radius a is brought to the position $z=h$ inside this evanescent field, it scatters the evanescent wave with an intensity which is $I_0' e^{-\xi(h-a)}$, see Refs. 23, 24. Thus the scattered intensity, which fluctuates owing to Brownian motion, determines sensitively and instantaneously the wall–colloid distance h. In order to obtain the spatial dependence of the potential energy of the particle one has to measure the separation distances sampled by the colloidal sphere for a statistically long period of time. From this, the probability distribution of finding the particle at any separation distance can be calculated which is directly related to the potential energy via the Boltzmann distribution. To determine the origin of the distance scale, we have referred the measured intensities to the scattering intensity of a particle that stuck to the substrate.

Since the experimental setup, see Fig. 2, is similar to that described earlier,[31] we will refer to the technical issues here only in brief. As a light source we used a 10 mW HeNe laser with a wavelength of $\lambda=633$ nm. The angle of incidence was chosen in a way that the characteristic decay length ξ of the evanescent field was 250 nm. The sample cell which was composed of two parallel optical flats of silica with an O-ring in between was optically matched to a glass prism. In order to control the salt concentration in the cell, it was connected to a closed circuit with Teflon tubes. This circuit contained also a conductivity meter, a storage container, a peristaltic pump and a vessel with ion exchange resin which allowed to control the Debye length in the system.[32] As particles we used surfactant free monodisperse polystyrene (PS) latex spheres[25] of 10 μm diam and 3 μm diam silica spheres[26] which were suspended in water. In order to guarantee that only a single particle was in the field of view during the measurement, only highly diluted suspensions were used. Prior to the measurement the solution was completely deionized corresponding to a conductivity of 0.07 μS/cm which is close to the theoretically expected value of pure water.

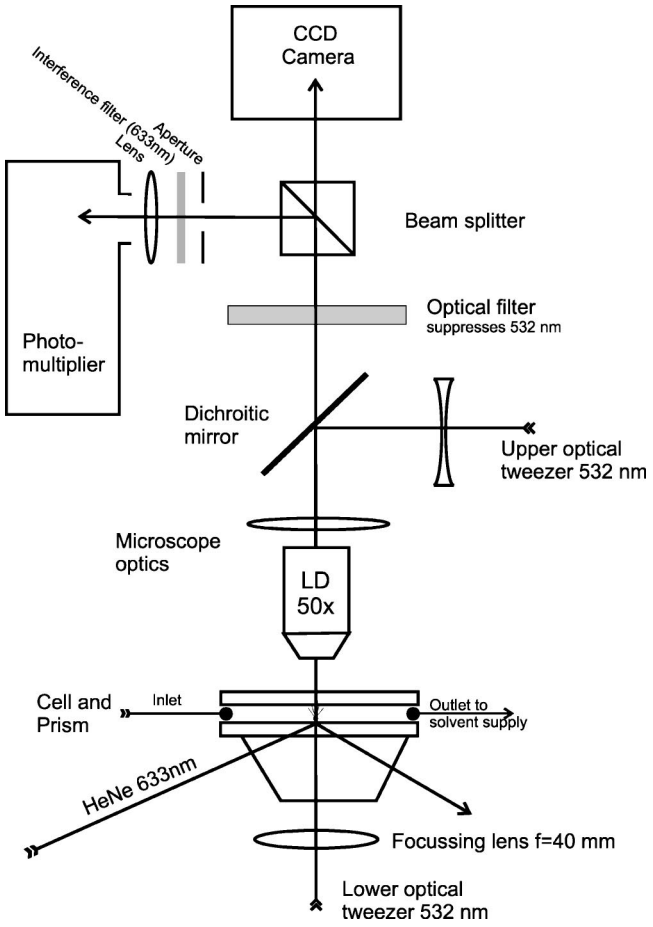

FIG. 2. Sketch of the experimental setup. The scattered light of the colloid is imaged onto a CCD camera and focused onto a photomultiplier by a microscope optics. An upper and a lower optical tweezer are focused by additional lenses on the particle and serve to manipulate the colloid.

In addition to our conventional TIRM-setup we used two optical tweezers[27] which were directed onto the particle from the top and the bottom of the cell, see Fig. 2. The idea of using light forces to control the movement of the particle has been introduced to the TIRM method by Brown *et al.*[28] and Walz *et al.*[29] In our case both tweezers were formed by a 200 mW frequency doubled Nd:YAG laser ($\lambda=532$ nm). As the upper tweezer we employed a strongly focused laser beam with an adjustable intensity of 50–150 mW. This tweezer served to hold the particle tightly in the view-field while exchanging the solvent in the sample cell and allowed us to perform measurements at different salt concentration with the same particle. The other optical tweezer coming from the bottom was only moderately focused by an $f=40$ mm lens and operated at much weaker intensities <200 μW. It only served to restrict the lateral movement of the particle during the measurement but was too weak to induce a noticeable vertical light pressure on the particle. The latter was confirmed by measuring potentials at various laser intensities and comparing them to measurements without the tweezer. Measurements at different salt concentrations were performed by adding small amounts of NaCl solutions to the

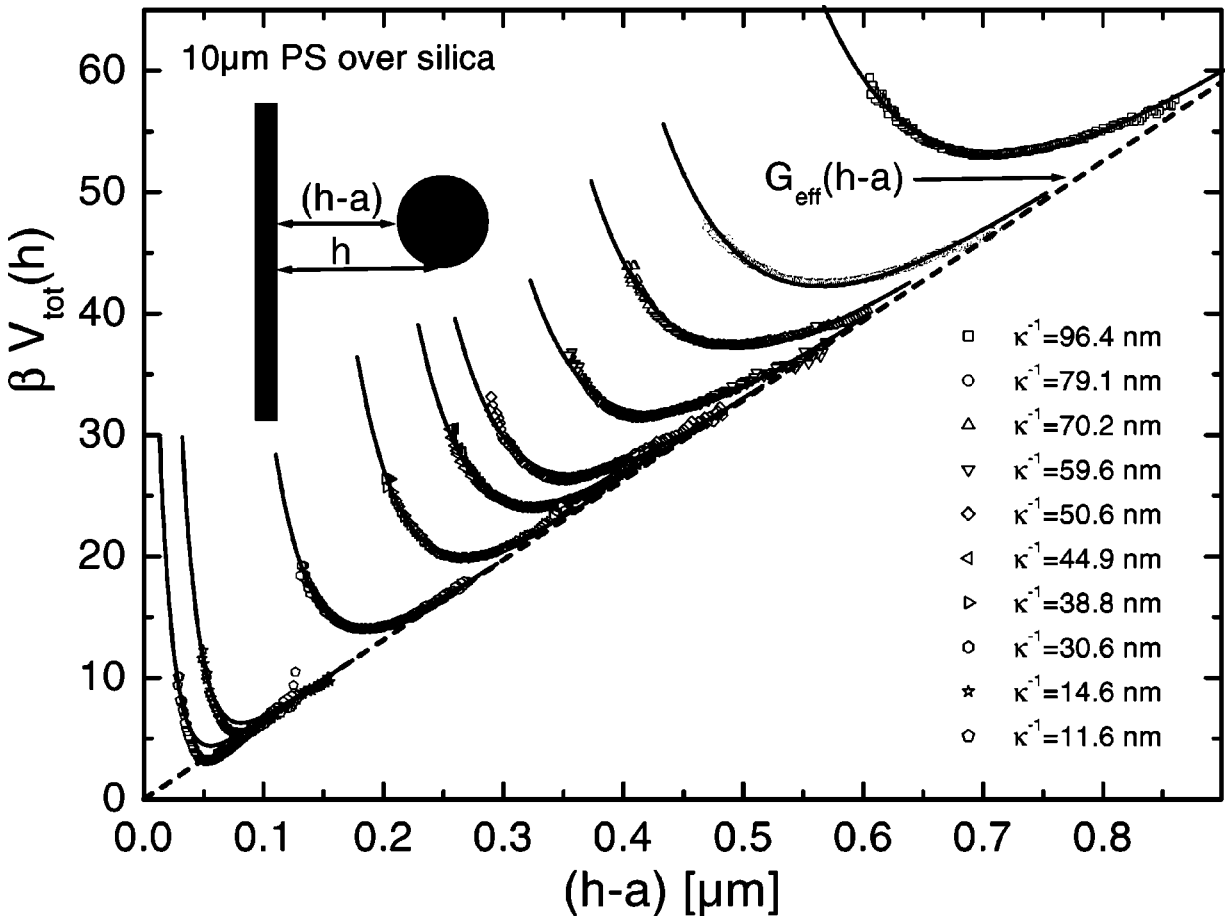

FIG. 3. Total interaction energy $\beta V_{\mathrm{tot}}(h)$ for a 10 μm charged polystyrene (PS) particle in front of a silica surface as obtained by TIRM. Plotted are the measured interaction potentials $\beta V_{\mathrm{tot}}(h)$ as a function of the wall–particle distance $h-a$, for ten different salt concentrations between $\kappa^{-1}=10$ nm and $\kappa^{-1}=100$ nm (symbols). Since each potential is a sum of a κ-dependent double-layer contribution at short distances and a κ-independent gravitational contribution at larger distances, all potentials approach the same limiting straight line (dashed) given by $G_{\mathrm{eff}}(h-a)$. Fitted curves (solid lines) are $\beta V_{\mathrm{fit}}(h)$ as explained in the text.

circuit and gently pumping until the conductivity meter indicated a constant distribution of the salt. The value of the conductivity meter agreed to the amount of added salt and allowed to calculate the Debye screening length within an error of 5%. After equilibration the upper optical tweezer was turned off and the particle was held in the middle of the field of view during the measurement with the lower tweezer. In order to exclude effects due the possible inhomogeneity of the substrate, all potentials were measured at the same position over the substrate.

IV. RESULTS AND DISCUSSION

Figure 3 displays the measured total potentials βV_{tot}, i.e., the sum of Eqs. (17), (18), and (19), for the 10 μm PS sphere, for ten different Debye lengths ranging between 10 nm and 100 nm. At higher salt concentrations the particles stick to the surface due to attractive dispersion forces. All potentials have a very similar shape: towards larger distances they increase linearly, because gravity is the dominant force acting on the particle [Eq. (17)]. At smaller distances repulsive double-layer interaction and attractive dispersion forces between the particle and the wall become important. The vertical position of the potentials are not known *a priori* since TIRM determines potentials relative to an arbitrary reference value. However, since at very large distances double-layer forces are insignificant, all potentials in Fig. 3 have to converge to the sheer gravitational contribution [Eq. (17)]

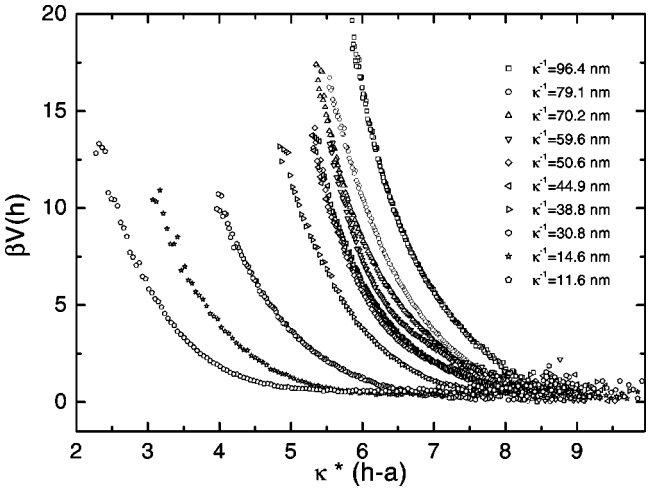

FIG. 4. Effective double-layer potentials between a glass surface and a PS sphere, obtained from the data in Fig. 3 by subtracting κ-independent contributions due to dispersion and gravitation forces.

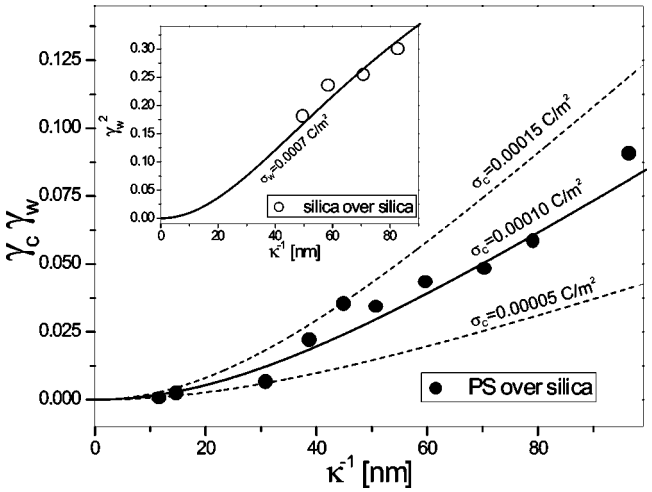

FIG. 5. Prefactors B in the function $Be^{-\kappa(h-a)}$, as obtained from a fit to data like those of Fig. 4. Values for B are divided by $16a/\lambda_B$ so as to facilitate a direct comparison to the theoretical function $\gamma_W\gamma_C$ over κ^{-1} in Eq. (11) (plotted as solid line). Shown are data for a PS sphere over silica, and for a silica sphere over silica (inset figure). To demonstrate how sensitive our method is, the function $\gamma_W\gamma_C$ is plotted for three values of the colloidal surface charge density, $\sigma_C=0.00005$, $\sigma_C=0.0001$, and $\sigma_C=0.00015$.

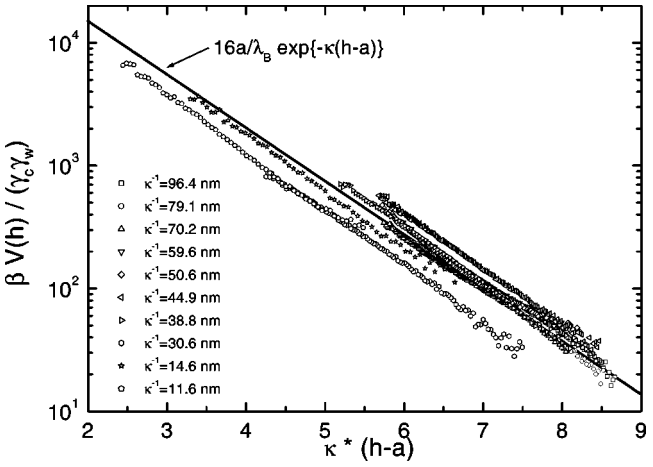

FIG. 6. Potentials of Fig. 4 divided by $\gamma_w\gamma_c$ in a logarithmic plot. All potentials collapse on the simple function $16ae^{-\kappa(h-a)}/\lambda_B$ (solid straight line).

which is plotted as a dashed line. Accordingly, if the potentials are fitted to the function $\beta V_{\rm disp}(h)+\beta V_{\rm fit}(h)$ with $\beta V_{\rm disp}(h)$ from Eq. (18) and $\beta V_{\rm fit}(h)=Be^{-\kappa(h-a)}+G_{\rm eff}(h-a)+\beta V_0$ using B and βV_0 as fit parameters, then the values of V_0 can be used to relate the vertical positions of the potentials with respect to each other. Further below the κ dependence of B is discussed in detail.

As expected, the mean colloid–wall distance decreases with decreasing Debye length. In addition we observe that the left branch of each potential becomes steeper with decreasing Debye length, a feature that is to be expected from the exponential of Eq. (19). To show that dispersion forces here play a rather marginal role, we compare our data not with $\beta V_{\rm disp}(h)+\beta V_{\rm fit}(h)$, but with the functions $\beta V_{\rm fit}(h)$ (solid lines in Fig. 3). For $\kappa^{-1}\geqslant 30.6$ nm, the solid curves of the function $\beta V_{\rm fit}(h)$ lie always on top of the data, and it is thus clear that the dispersion forces are insignificant for this distance regime. Only for the two curves closest to the wall, a small difference between $\beta V_{\rm fit}(h)$ and the data can be observed. This now shows the contribution of the dispersion forces, which is obviously small compared to all other contributions. Plotting $\beta(V_{\rm disp}(h)+V_{\rm fit}(h))$, we would obtain curves that coincide also for the two curves closest to the wall.

Since in the following we will concentrate on the double-layer repulsion, we subtracted gravitation and dispersion contributions from our data, i.e., Eqs. (17) and (18) which contain no open parameter. As a result, we obtain Fig. 4 with the bare double-layer potentials, plotted as a function of $\kappa(h-a)$. Provided that Eq. (19) is the correct potential, we expect the experimental potentials to have all the same exponential factor $\exp(\kappa(h-a))$. If this were the only κ dependence of the double-layer potential, all curves in Fig. 4 should fall on one common curve. However, as is evident from the plot, this is not the case: Obviously the prefactor also depends on κ, and looking back to Eqs. (19) and (11), we realize that this additional κ dependence arises from the κ dependence of the two γ factors. In the following we use this κ dependence to determine surface charge densities.

To proceed we divided the prefactors obtained from fitting the curves in Fig. 3 by $16a/\lambda_B$ and plotted them in Fig. 5 as a function of κ^{-1}. According to Eq. (19), our data should be described by the function $\gamma_W(\kappa^{-1})\gamma_C(\kappa^{-1})$ [both dependent on κ^{-1}, see Eq. (11)]. Using σ_W and σ_C in Eq. (11) as adjustable fitting parameters, we could in principle fit these data points to the function $\gamma_W(\kappa^{-1})\gamma_C(\kappa^{-1})$. This, however, would lead to surface charge densities with large error bars, and it would not be clear, which of the obtained σ values one has to attribute to the wall and which to the colloid. Alternatively, we replaced the PS spheres by particles made of the same material as the glass surface, i.e., silica, because then, $\gamma_W(\kappa^{-1})$ and $\gamma_C(\kappa^{-1})$ are identical which simplifies the problem to a single fitting parameter. The resulting surface charge density of the silica surface can then be used for the analysis of the PS data. We used 3 μm silica spheres, and analyzed the data in the same way as described above. The result is plotted as open symbols in the inset of Fig. 5. Fitting these four points to the function $\gamma_W^2(\kappa^{-1})$ given in Eq. (11), we determine the surface charge density of the wall to $\sigma_W=0.0007$ C/m^2. Inserting this value in Eq. (11), we obtain the solid line in the inset of Fig. 5. This value is in excellent agreement with those obtained by Dunstein[30] from electrophoresis measurements, who found a surface charge density of $\sigma_W=0.000\,65$ C/m^2.

With the knowledge of γ_W, we now can determine the surface charge density of the PS spheres using Eq. (11) to $\sigma_C=0.0001$ C/m^2. The fitted curve $\gamma_W\gamma_C$ from Eq. (11) is displayed in Fig. 5 as a solid curve. To demonstrate how sensitive our method is, we have added two curves of the same function with $\sigma_C=0.000\,15$ C/m^2 and $\sigma_C=0.000\,05$ C/m^2. The theoretical and experimental data show in particular at higher values of κ^{-1} good agreement and indicate that in both experiments (PS and silica spheres) our data can be well described by Eq. (11). We conclude that

with the method proposed here, surface charge densities can be determined within $\pm 30\%$ roughly.

The agreement observed in Fig. 5 also implies that our measurements are in good agreement with the theoretical double-layer potential of Eq. (19). This can be seen by dividing the potentials of Fig. 4 each by its value of $\gamma_W \gamma_C$ which is a quantity known now for every κ. It follows from Eq. (19) that the potentials scaled in this way, should all have the same prefactor $16a/\lambda_B$. In a semilogarithmic representation, this means that all curves should appear as straight lines having the same slope and intersection. This is indeed confirmed by Fig. 6, where we see all potentials collapsing onto one common master-curve. This proves that Eq. (19) correctly describes the double-layer interaction between the wall and the colloid. The small deviations of the experimental data from the master curve are attributed to an approximate error of 5% in the κ-values derived from our ionic conductivity measurements. Another possible systematic error enters through the determination of γ_W because it was assumed that the surface potentials of the silica substrate and the silica bead are equal. Even if the same material is used, it is possible that differences in the nanoscopic surface structure of the optically polished substrate and the 3 μm bead can cause differences in the surface charge density. The surface charge densities found for the PS sphere are of the same order of magnitude as for silica. Since the surface charge of PS strongly depends on the details of the production process, we cannot compare our result to the values found in literature. Relating information on the surface charge density has not been released by the manufacturer.[25]

Finally, we would like to make some general remarks on the TIRM method and how it compares to conventional methods. The reason, TIRM achieves a higher resolution in force measurements than conventional AFM is largely due to the fact, that during TIRM experiments the system remains under equilibrium conditions. Only then, the particle fluctuations allow the precise determination of the potential energy. In contrast, during an AFM measurement, a piezo exerts a force onto a cantilever which then leads to nonequilibrium conditions. To obtain the force in an AFM experiment, one has to measure the bending of the cantilever (e.g., by a light-deflection method). The accuracy of such a measurement, however, is limited by thermal fluctuations which tend to disturb the signal and thus limit the force resolution to about 50 pN in conventional AFM.[36] The resolution of TIRM, on the other hand, has been demonstrated to be as low as 10 fN, see Ref. 37. It should be mentioned, that very recently the basic idea of using thermal fluctuations to obtain surface potentials has been also applied to AFM.[38] It has been demonstrated that if a tip is brought close to a surface immersed in an electrolyte, its movement is governed by the sum of the harmonic cantilever potential and the tip–surface interaction.

To compare our method to the ζ-potential measurements of surface potentials, we have to recall that the surface charge is created by ionized surface groups and by ions tightly adsorbed in the Stern layer.[6] The plane of closest approach of the ions from the diffuse part of the electrical double-layer is called the outer Helmholtz plane (OHP). All ions on the wall-faced side of the OHP make up the surface-charge density σ_W. To be distinguished from the OHP is the shear plane which separates the hydrodynamically immobile liquid that moves together with the surface from the mobile liquid which has nonzero relative velocity with respect to the surface. The ζ-potential refers to this shear plane and is thus an useful approximation to the real surface potential only if the OHP lies sufficiently close to the shear plane. That, however, is not known. In our TIRM method, on the other hand, the position of the shear plane is insignificant. One might argue that also in our experiment, one cannot be sure if one measures the ''true'' surface charge density right at the OHP or an apparent surface charge density at any other plane. However, the distinction between true and apparent charges is of no importance, as long as we deal with those charges that determine the physical properties of the colloidal suspension, i.e., those that are relevant to such effects as the formation of colloidal crystals, wall crystallization or the stability of dispersions. These charges are, indeed, what we have measured by the TIRM method proposed here; its main advantage thus lies in the fact that it measures an dynamically unperturbed double-layer in equilibrium.

The BVP in Eq. (3) is set up using constant-charge boundary conditions. Likewise, the effective interaction potentials—the numerical one as well as the analytical one in Eq. (19)—are based on the assumption that the surface charge density on both wall and colloid is a constant and does not depend on the salt content of the electrolyte. In principle, there are two different ways by which the charge density at the surfaces can be affected: by adsorption of either H^+ or Na^+ cations. Since the experiments were performed at fixed $p\mathrm{H}(p\mathrm{H}=6.5\pm 0.5)$ for all κ values, the degree of dissociation of the surface groups is always the same. In fact, at the pH value chosen here, the sulfate groups at the PS surface are completely dissociated.[39] Quite another point is the adsorption of cations onto the surfaces; while this is likely to be true for polyvalent ions,[1] it seems to be rather unlikely in case of the monovalent salt ions chosen in our experiment. Therefore, the assumption of a κ-independent surface charge density is fulfilled to a good approximation.

Finally, we want to mention that the data plots of Fig. 4 can also be regarded as an indirect measurement of the old Gouy–Chapman potential, Eqs. (9) and Eq. (12). We have seen that the potential of Eq. (19) is the product of the effective colloidal charge $Z_{\mathrm{eff}}=-4a\gamma_C e^{\kappa a}/\lambda_B$, see Eq. (14), and the Gouy–Chapman potential $\Phi_1(z)=-4\gamma_W e^{-\kappa z}$ in Eq. (12), and can thus be understood as resulting from the interaction of a point-charge of effective charge Z_{eff} with the unperturbed Gouy–Chapman layer. The colloidal sphere is therefore nothing but the ''test charge'' by means of which we have probed the Gouy–Chapman potential, and devision of the data in Fig. 4 by the charge of this test particle results in data measuring directly the famous Gouy–Chapman potential.

V. SUMMARY

A double-layer in front of a planar wall that has a surface charge density of σ_W, creates a electrostatic mean-field potential of $-4\gamma_W e^{-\kappa z}$, where γ_W is a complicated function of σ_W/κ [Eq. (11)]. Probing this potential with a colloidal

test charge at $z=h$ that itself has a double layer gives another γ_C factor and one arrives at an interaction potential that goes with $\gamma_C\gamma_W e^{-\kappa h}$. The product $\gamma_C\gamma_W$ depends on σ_W/κ and σ_C/κ, i.e., on the surface charge densities of the colloidal test charge and the wall. In this paper, we have carried out an accurate TIRM measurement of the wall–colloid interaction potential for a sequence of different Debye-lengths, and thus determined $\gamma_C\gamma_W$ as a function of κ^{-1}. We have done that for two types of colloidal particles, silica and polystyrene, and found good agreement between the experimental data and the theoretical prediction for the function $\gamma_C\gamma_W$, with σ_W and σ_C being the only two fit parameters. We have discussed the numerical values of the obtained surface charge densities, and showed that they are in accord with one's expectation.

The functional dependence of the colloid–wall interaction potential has been measured with TIRM before. Here, we took the κ dependence of the prefactor of the exponentially decaying double layer repulsion explicitly into account which then leads to a precise determination of surface charges. In the standard TIRM-data evaluation,[10–12] however, this dependence is neglected, because the prefactor of Eq. (19) is typically expressed in terms of the position of the potential minimum formed by double layer and gravitational forces. If that is done the dependence on the surface charges σ_W and σ_C is eliminated from the data, and valuable information about the surface is lost.

ACKNOWLEDGMENTS

We gratefully acknowledge the help of Christoph Lutz in introducing the optical tweezer in the setup and the financial support from the Deutsche Forschungsgemeinschaft through SFB 513 and the Optikzentrum Konstanz.

APPENDIX A: LINEAR THEORY

In the following we derive Eq. (7), i.e., an approximate expression for the effective wall-sphere potential, from Eqs. (3) and (5). Let us consider the case when both the colloidal and the interfacial charge density is small enough for Φ to be everywhere smaller than one. This allows us to linearize the PB equation, i.e., to replace $\sinh\Phi$ in Eq. (3) by Φ. Since the resulting Helmholtz equation is a linear equation, we can split the BVP of Eq. (3) into two separate BVP's, namely, a BVP for a potential Φ_1,

$$\begin{aligned}
&\nabla^2\Phi_1(\mathbf{r})=\kappa^2\Phi_1(\mathbf{r}), && \mathbf{r}\in G,\\
&\mathbf{n}_W\nabla\Phi_1=4\pi\lambda_B\sigma_W, && \mathbf{r}\in\partial G_W,\\
&\mathbf{n}_C\nabla\Phi_1=0, && \mathbf{r}\in\partial G_C,
\end{aligned} \tag{A1}$$

and one for a potential Φ_2,

$$\begin{aligned}
&\nabla^2\Phi_2(\mathbf{r})=\kappa^2\Phi_2(\mathbf{r}), && \mathbf{r}\in G,\\
&\mathbf{n}_W\nabla\Phi_2=0, && \mathbf{r}\in\partial G_W,\\
&\mathbf{n}_C\nabla\Phi_2=4\pi\lambda_B\sigma_C, && \mathbf{r}\in\partial G_C.
\end{aligned} \tag{A2}$$

It is evident that the sum of these two BVP's again result in the original BVP of Eq. (3) (in its linearized form), and that the solution Φ can accordingly be obtained from the sum of Φ_1 and Φ_2.

What effect has the linearization approximation on the grand potential, Eq. (5)? Using Green's first identity to transform the volume integral over $\nabla\Phi^2$ in Eq. (5) into a surface integral plus a volume integral and realizing furthermore that $\Phi\sinh\Phi-2(\cosh\Phi-1)\approx 0$ if $\Phi<1$, we obtain

$$\beta\Omega=\frac{1}{8\pi\lambda_B}\left[\int_{\partial G_W}d\mathbf{S}\cdot\nabla\Phi\Phi+\int_{\partial G_C}d\mathbf{S}\cdot\nabla\Phi\Phi\right]-\beta W^{\mathrm{SE}}, \tag{A3}$$

which by using the boundary conditions of Eq. (3) reduces to

$$\beta\Omega=-\frac{\sigma_W}{2}\int_{\partial G_W}dS\Phi-\frac{\sigma_C}{2}\int_{\partial G_C}dS\Phi-\beta W^{\mathrm{SE}}. \tag{A4}$$

We thus see that, in linear theory, the grand potential reduces to just the electrostatic energy of the system, that is the energy which the colloidal (σ_C) and interfacial charges (σ_W) have in the mean-field potential Φ. Placing now the sum $\Phi=\Phi_1+\Phi_2$, with Φ_1 from the BVP of Eq. (A1) and Φ_2 from the BVP of Eq. (A2), into Eq. (A4), we find

$$\begin{aligned}
\beta\Omega=&-\frac{\sigma_W}{2}\int_{\partial G_W}dS(\Phi_1+\Phi_2)\\
&-\frac{\sigma_C}{2}\int_{\partial G_C}dS(\Phi_1+\Phi_2-\Phi_0),
\end{aligned} \tag{A5}$$

where $\Phi_0=-Z\lambda_B/((z-h)^2+s^2)^{1/2}$ is the bare Coulomb potential of the Z colloidal charges, which, when integrated over the colloid surface and multiplied by $\sigma_C/2$, results in the self-energy $\beta W^{\mathrm{SE}}=Z^2\lambda_B/2a$. (Since there is still a rotational symmetry about the line joining the centers of the colloidal particle and its image, we have two spatial variables in our problem. These variables are z and s, with z being the coordinate along this symmetry line, and s perpendicular to it.)

The energy of the colloidal charges in the potential produced by the wall surface charges equals the energy of the wall charges in the potential due to the colloidal charges. Therefore, $\sigma_W\int_{\partial G_W}dS\Phi_2=\sigma_C\int_{\partial G_C}dS\Phi_1$, by means of which Eq. (A5) can be further simplified to

$$\beta\Omega=-\frac{\sigma_W}{2}\int_{\partial G_W}dS\Phi_1-\frac{\sigma_C}{2}\int_{\partial G_C}dS(2\Phi_1+\Phi_2-\Phi_0). \tag{A6}$$

This expression is used further down to derive the interaction potential.

Let us now discuss the solution of the BVP's in Eqs. (A1) and (A2). With Eq. (A1), we have formulated the BVP for an uncharged colloidal sphere of vanishing dielectric constant brought into and thus perturbing the ion double-layer of a charged wall. We neglect these steric effects and assume in the following that this perturbation has little effect on our results, which is equivalent to ignoring the second boundary condition in Eq. (A1) (a good approximation for reasonably large h). The solution of Eq. (A1) then is

$$\Phi_1(z) = -4\pi \frac{\lambda_B \sigma_W}{\kappa} e^{-\kappa z}. \tag{A7}$$

The second BVP, Eq. (A2), is more difficult to solve. Only in the limit $\kappa a \to 0$, there exists an analytical solution,[40]

$$\Phi_2^h(s,z) = -Z\lambda_B \kappa \int_0^\infty dl J_0(\kappa s l) \frac{l}{\tilde{l}} (e^{-\kappa|z-h|\tilde{l}} + e^{-\kappa(z+h)\tilde{l}}), \tag{A8}$$

with $\tilde{l} = (1+l^2)^{1/2}$ and J_0 being the Bessel function of the first kind.

Note that Φ_2^h depends on the position of the colloid while Φ_1 in our approximation does not. Returning now to Eq. (A6), we recognize that, due to this independence, the first term of Eq. (A6) drops out when we calculate $\beta V(h) = \beta(\Omega_h - \Omega_\infty)$. In the limit $\kappa a \to 0$, the interaction potential then becomes

$$\beta V(h) = -\frac{Z}{2}(2\Phi_1 + \Phi_2^h - \Phi_0^h)|_{z=h,s=0}^{z=\infty,s=0}, \tag{A9}$$

which by using Eq. (A8) reduces to[18]

$$\beta V(h) = -Z\Phi_1(z)|_{z=\infty}^{z=h} + \frac{Z^2 \lambda_B}{2} \frac{e^{-2\kappa h}}{2h}, \tag{A10}$$

where Φ_1 is the potential given in Eq. (A7).

APPENDIX B: ALTERNATIVE DERIVATION OF THE INTERACTION POTENTIAL

It is instructive to recall the conventional way to derive the interaction potential of Eq. (19), given, for example, in the book of Verwey and Overbeek.[13] We first consider the interaction of a sphere and a wall, both made of the same material and having the same surface charge density, when exposed to an aqueous electrolyte solution. Let us begin by writing down the free energy per area $\beta F/A_{\text{rea}}$ for two parallel plates made of this material. If these plates are a distance $2D$ apart from each other, then

$$\beta F(2D)/A_{\text{rea}} = 2\int_D^\infty p(x)dx, \tag{B1}$$

where $p(x)$ is the pressure in the electrolyte solution when the plates have a relative distance of $2x$. The pressure of the system in such a symmetric case, can most easily be calculated at the midplane between both plates, because there the electric field must be zero, and the pressure then is nothing but the osmotic pressure, namely the sum of $\rho_+ = \rho_s e^{-\Phi}$ and $\rho_- = \rho_s e^{\Phi}$ minus two times the bulk pressure. Hence, $\beta p = 2\rho_s(\cosh(\Phi_{\text{mid}}) - 1)$. If the interaction is small, the electric potential due to one double layer will be negligible at the surface of the second plate. We may therefore assume that the electric potential in the neighborhood of the midplane is built up additively from the electric potentials due to the two unperturbed double layers separately, which we know from Eq. (12) to be $\Phi(z) = -4\gamma e^{-\kappa z}$ with $\kappa = 8\pi\lambda_B \rho_s$. Therefore,

$$\Phi_{\text{mid}} = -8\gamma e^{-\kappa z}, \tag{B2}$$

if the plates are a distance $2x$ apart from each other. As we have assumed that the interaction is small, the electric potential midway between the plates will also be small, so that $\Phi_{\text{mid}} < 1$. Therefore, the pressure is approximately,

$$\beta p(x) = 2\rho_s(\cosh(\Phi_{\text{mid}}) - 1) \approx \rho_s \Phi_{\text{mid}}^2. \tag{B3}$$

Inserting this in Eq. (B1) and performing the integral gives

$$\beta F(2D)/A_{\text{rea}} = 64\rho_s \gamma^2 \frac{e^{-2\kappa D}}{\kappa}. \tag{B4}$$

To come from this plate-plate free energy to the effective sphere–plate interaction, we have to make use of the Derjaguin approximation,[1] leading to

$$\beta V(h) = 2\pi a \int_{h-a}^\infty \beta F(y)/A_{\text{rea}} dy = \frac{16a}{\lambda_B} \gamma^2 e^{-\kappa(h-a)}, \tag{B5}$$

which is the interaction potential of Eq. (19). We thus see that it is based not only on the Derjaguin approximation, but also one the assumption that two unperturbed Gouy–Chapman solutions for isolated walls can be superposed to describe the electric potential between parallel plates.

If the surface charge density of the sphere differs from that of the plate, i.e., if $\gamma_W \neq \gamma_C$, this derivation must be modified. The problem is that the electric field at the midplane is no longer zero, but contributes to the pressure. An alternative way is to calculate $\beta F/A_{\text{rea}}$ by

$$\beta F(2D)/A_{\text{rea}} = -\sigma'_W \Phi_C(2D) - \sigma'_C \Phi_W(2D), \tag{B6}$$

which is the electrostatic energy of the colloidal charges in the double layer potential of an isolated wall and vice versa, $\Phi_{W/C} = -4\gamma_{W/C} e^{-\kappa 2D}$. To account for the entropic contributions of the microions to the free energy, we have to take the apparent surface charge density $\sigma'_{W/C}$ instead of the real. The latter we obtain by identifying the potential in linearized form Eq. (A7), $\Phi_{W/C}^{\text{in}} = -4\pi\lambda_B \sigma'_{W/C} e^{-\kappa 2D}/\kappa$ with $\Phi_{W/C} = -4\gamma_{W/C} e^{-\kappa 2D}$, from which we obtain

$$\sigma'_{W/C} = \frac{\kappa \gamma_{W/C}}{\pi \lambda_B}. \tag{B7}$$

The free energy per area then becomes

$$\beta F(2D)/A_{\text{rea}} = \frac{8\kappa\gamma_W\gamma_C}{\pi\lambda_B} e^{-\kappa 2D} = 64\rho_s \gamma_W \gamma_C \frac{e^{-2\kappa D}}{\kappa}, \tag{B8}$$

from which we finally obtain

$$\beta V(h) = 2\pi a \int_{h-a}^\infty \beta F(y)/A_{\text{rea}} dy = \frac{16a}{\lambda_B} \gamma_C \gamma_W e^{-\kappa(h-a)}. \tag{B9}$$

[1] J. Israelachvili, *Intermolecular and Surface Forces* (Academic, London, 1992).

[2] D. F. Evans and H. Wennerström, *The Colloidal Domain: Where Physics, Chemistry, Biology, and Technology Meet* (VCH, New York, 1994).

[3] H. Löwen and J. P. Hansen, Annu. Rev. Phys. Chem. **51**, 209 (2000).

[4] J. M. Kleijn and H. P. van Leeuwen, in *Physical Chemistry of Biological Interfaces*, edited by A. Baszkin and W. Norde (Marcel Dekker, New York, 2000).

[5] H. Lekkerkerker, Physica A **159**, 319 (1989); Barneveld *et al.*, Langmuir **10**, 1084 (1994).

[6] K. S. Birdi, *Handbook of Surface and Colloid Chemistry* (CRC, New York, 1997).
[7] W. A. Ducker, T. J. Senden, and R. M. Pashley, Nature (London) **353**, 239 (1991).
[8] R. M. Pashley, Sci. Prog. **78**, 173 (1995), and references therein.
[9] V. S. J. Craig, A. M. Hyde, and R. M. Pashley, Langmuir **12**, 3557 (1996).
[10] D. C. Prieve, Adv. Colloid Interface Sci. **82**, 93 (1999).
[11] J. Y. Walz, Curr. Opin. Colloid Interface Sci. **2**, 600 (1997).
[12] S. G. Bike, Curr. Opin. Colloid Interface Sci. **5**, 144 (2000).
[13] E. J. W. Verwey and J. T. G. Overbeek, *Theory of the Stability of Lyophobic Colloids* (Elsevier, Amsterdam, 1948).
[14] G. Gouy, J. Phys. (Paris) **9**, 457 (1910); D. L. Chapman, Philos. Mag. **25**, 475 (1913).
[15] J. L. Barrat and J. F. Joanny, Adv. Chem. Phys. **94**, 1 (1996).
[16] H. H. von Grünberg and E. C. Mbamala, J. Phys.: Condens. Matter **12**, 10349 (2000).
[17] Depending on σ_W and the distance of the colloidal sphere from the wall, they can become more important than the interfacial charges. Consider, for instance, the case $\sigma_W=0$. We see from Eq. (2) that in this case the normal component of the electric field at $z=0$ must vanish, which for symmetry reasons is only possible if the charge distribution at $z>0$ has a perfect mirror image at $z<0$. So, in this limit, the potential will be dominated solely by the image charges.
[18] H. H. von Grünberg and E. C. Mbamala, J. Phys.: Condens. Matter (in press).
[19] Noteworthy is also the factor 1/2 in front of the second term which does not appear if one considers the screened interaction between two real point-charges having the same relative distance in a bulk system. It arises from the fact that at $z=-h$ there is an image charge and not a real charge (the interaction between two real charges at a distance d is $Z^2\lambda_B/d$, while the interaction between a real charge and its own image charge at the same relative distance is only $Z^2\lambda_B/2d$).
[20] S. Alexander, P. M. Chaikin, P. Grant, G. J. Morales, P. Pincus, and D. Hone, J. Chem. Phys. **80**, 5776 (1984).
[21] L. Belloni, Colloids Surf., A **140**, 227 (1998).
[22] M. A. Bevan and D. C. Prieve, Langmuir **15**, 7925 (1999).
[23] D. C. Prieve and J. Y. Walz, Appl. Opt. **32**, 1629 (1993).
[24] C. Liu, T. Kaiser, S. Lange, and G. Schweiger, Opt. Commun. **117**, 521 (1995).
[25] Catalog Number 4210A from Duke Scientific Corporation, Palo Alto, CA 94303; actual diameter 9.975 ± 0.061 μm.
[26] Catalog Number SS05N/004181 from Bangs Laboratories, Inc., Fishers, IN 46038-2886; actual diameter 2.990 ± 0.080 μm.
[27] A. Ashkin, Biophys. J. **61**, 569 (1992).
[28] M. A. Brown, A. L. Smith and E. J. Staples, Langmuir **5**, 1319 (1989).
[29] J. Y. Walz and D. C. Prieve, Langmuir **8**, 3073 (1992).
[30] D. E. Dunstain, J. Colloid Interface Sci. **166**, 472 (1994); the surface charge density $\sigma_C=0.00065\,\mathrm{C/m^2}$ for our experimental situation $T=25\,^\circ\mathrm{C}$ can be obtained by interpolating data points in Fig. 3.
[31] D. Rudhardt, C. Bechinger, and P. Leiderer, Phys. Rev. Lett. **81**, 1330 (1998).
[32] T. Palberg, W. Härtl, W. Wittig, H. Versmold, M. Würth, and E. Simnacher, J. Phys. Chem. **96**, 8180 (1992).
[33] S. G. Bike and D. C. Prieve, Int. J. Multiphase Flow **16**, 727 (1990).
[34] S. G. Flicker and S. G. Bike, Langmuir **9**, 257 (1993).
[35] S. G. Flicker, J. L. Tipa, and S. G. Bike, J. Colloid. Interface Sci. **158**, 317 (1993).
[36] A. Milling and S. Biggs, J. Colloid Interface Sci. **170**, 604 (1995).
[37] D. Rudhardt, C. Bechinger, and P. Leiderer, J. Phys.: Condens. Matter **11**,10073 (1999).
[38] O. H. Willemsen, L. Kuipers, K. O. v. d. Werf, B. G. d. Grooth, and J. Greve, Langmuir **16**, 4339 (2000).
[39] S. F. Schultz, T. Gisler, M. Borkovec, and H. Sticher, J. Colloid Interface Sci. **164**, 88 (1994).
[40] F. H. Stillinger, J. Chem. Phys. **35**, 1584 (1961).